International Journal of Biological Macromolecules 278 (2024) 134845

Contents lists available at ScienceDirect

International Journal of Biological Macromolecules

journal homepage: www.elsevier.com/locate/ijbiomac

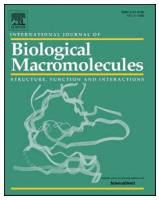

Serum protein albumin and chromium: Mechanistic insights into the interaction between ions, nanoparticles, and protein

Zoltan Wolfgang Richter-Bisson [a,*], Heng-Yong Nie [b,c], Yolanda Susanne Hedberg [a,b,d,*]

[a] Department of Chemistry, Western University, London, ON N6A 5B7, Canada
[b] Surface Science Western, Western University, London, ON N6G 0J3, Canada
[c] Department of Physics and Astronomy, Western University, London, ON N6A 3K7, Canada
[d] Lawson Health Research Institute, London, ON N6C 2R5, Canada

ARTICLE INFO

Keywords:
Corrosion
Nanoparticles
Protein corona
Protein aggregation
Chromium (Cr)
Bovine serum albumin (BSA)
Time-of-flight secondary ion mass spectrometry (ToF-SIMS)

ABSTRACT

The interaction of human proteins and metal species, both ions and nanoparticles, is poorly understood despite their growing importance. These materials are the by-products of corrosion processes and are of relevance for food and drug manufacturing, nanomedicine, and biomedical implant corrosion. Here, we study the interaction of Cr(III) ions and chromium oxide nanoparticles with bovine serum albumin in physiological conditions. This study combined electrophoretic mobility measurements, spectroscopy, and time-of-flight secondary ion mass spectrometry with principal component analysis. It was determined that neither metal species resulted in global albumin unfolding. The Cr(III) ions interacted strongly with amino acids found in previously discovered metal binding sites, but also were most strongly implicated in the interaction with negatively charged acid residues, suggesting an electrostatic interaction. Bovine serum albumin (BSA) was found to bind to the Cr_2O_3 nanoparticles in a preferential orientation, due to electrostatic interactions between the positive amino acid residues and the negative chromium oxide nanoparticle surface. These findings ameliorate our understanding of the interaction between trivalent chromium ions and nanoparticles, and biological macromolecules.

1. Introduction

The interactions between human proteins and metal remain poorly understood, even though they become increasingly important yearly. The utilization rate for arthroplasty implants has increased dramatically from the 1980s to the 2010s, and a report published by Data Horizons Research said the implantable medical device market is expected to grow at 7.3 % annually from 2024 to 2032, suggesting a dramatic increase in implantation rate. [1–3] A prevalent yet infrequently considered method of exposure to metal ions and metal nanoparticles (NP) is the corrosion of implanted biomedical devices such as arthroplasty implants or pacemakers, with nanoparticles being released in great quantities from malpositioned implants or implants undergoing a combination of both mechanical and chemical degradation (i.e. knee or hip implants). [4–10] Although both metal ions and nanoparticles are corrosion by-products, and both will be present in corrosion scenarios, they are known to interact very differently with macromolecules. When exposed to protein-rich environments, metal ions tend to cause proteins to aggregate. [11–13] When exposed to biological media, nanoparticles develop a dynamic coating of proteins called a protein corona. [14,15] Malfunctioning proteins, including these metal-protein aggregates, have been implicated in several health concerns, including metabolic dysfunction, allergies, pseudotumors, lesions, cancer, and neurodegenerative diseases. [8,16–24] This is a multi-faceted problem with implications for implant biomedical implant safety standards, food manufacturing, and for the developing field of nanomedicine, where nanoparticles are used as targeted-delivery drug carriers or as radiotherapy sensitizers for cancer treatments. [25,26]

Chromium (Cr) was chosen as the metal of interest due to its prevalence as an alloying element in two common biomaterials: the cobalt-chrome (CoCr) alloy and stainless steel. [27] The major metal ion released from corroding biomedical implants of this composition is the

Abbreviations: NP, nanoparticle; BSA, bovine serum albumin; HSA, human serum albumin; ToF-SIMS, time-of-flight secondary ion mass spectrometry; PCA, principal component analysis; CD, circular dichroism; MES, 2-(N-morpholino)ethanesulfonic acid; Tris, tris(hydroxymethane)aminomethane; cmPALS, continuously monitored phase analysis light scattering.

* Corresponding authors at: Department of Chemistry, Western University, London, ON N6A 5B7, Canada.
E-mail addresses: zrichter@uwo.ca (Z.W. Richter-Bisson), yhedberg@uwo.ca (Y.S. Hedberg).

https://doi.org/10.1016/j.ijbiomac.2024.134845
Received 1 August 2024; Received in revised form 14 August 2024; Accepted 16 August 2024
Available online 17 August 2024

trivalent form, Cr(III), not the highly carcinogenic Cr(VI). [10,28] For well-functioning implants, the majority of the wear debris is composed of chromium oxide (Cr_2O_3) nanoparticles (<100 nm), although malpositioned implants may release wear particles up to 1000 nm. [10] The physical characteristics of nanoparticles, such as size and charge, determine the nature of their interactions with proteins. It has been found that spherical nanoparticles tend to improve the binding affinity of proteins, a greater surface area results in more total protein binding and larger nanoparticles tend to bind intact proteins. In contrast, nanoparticles with a smaller radius of curvature tend to result in loss of protein secondary structure. [14]

Bovine serum albumin (BSA) was chosen as the protein of interest due to its 76 % structural homology with human serum albumin (HSA), low cost and wide availability. [29] Albumin proteins make up 60–65 % of mammalian blood, they are also found in the synovial fluid at roughly a third of the concentration in blood plasma, and skin. [30–33] These factors make albumin a highly desirable protein to study when exploring metal-induced protein aggregation.

Time-of-flight secondary ion mass spectrometry (ToF-SIMS) [34] was chosen due to its high surface sensitivity [35] (probing only 1–3 nm of the topmost surface), and because the measured spectra are rich in chemical information. All ions created in the sample analysis process are captured, which provides unique chemical selectivity for organic and biological materials via characteristic ions, providing valuable information regarding molecular conformation and surface chemical states or structures. ToF-SIMS is not quantitative due to matrix effects and variable ion yields from different species, so comparing different chemical species from one sample is impractical; however, comparing ion intensities of the same species or ion ratios of species among different samples is facile. [36] This makes it an ideal method for investigating and comparing the chemical motifs present in the interaction of BSA with Cr(III) ions and Cr_2O_3 nanoparticles. Due to its high sensitivity to chemical states and surfaces, ToF-SIMS has been used in combination with multivariate analysis such as principal component analysis (PCA) for detailed surface analysis of adsorbed protein layers. [37–43] PCA is a well-established form of multidimensional scaling that involves transforming variables into a lower-dimensional space while retaining a maximal amount of information about them. Principal components are essentially scaled, linear combinations of the original variables, and larger scores represent a larger percentage of the original variable behaviour. A full description of this process may be found elsewhere. [44,45]

This study aimed to identify the specific BSA amino acids that interact with Cr(III) ions and Cr_2O_3 nanoparticles to develop mechanistic insights for the documented phenomenon of Cr-induced protein aggregation. This was conducted using electrophoretic mobility measurements to determine the surface charge on Cr_2O_3 nanoparticles and BSA, circular dichroism (CD) spectroscopy to investigate protein unfolding, and ToF-SIMS for detailed information on protein chemical states.

2. Experimental

2.1. Chemicals and solutions

The solvent for all solutions was ultrapure (type 1) water purified with a Milli-Q Reference System (Millipore Sigma) to give a resistivity of 18.2 MΩ·cm. Cr_2O_3 (Chromium(III) oxide nanopowder, <100 nm particle size (TEM), 98 %, Sigma Aldrich, USA) nanoparticle suspensions were made at concentrations of 50 ppm in type 1 water, then tip sonicated (VWR Ultrasonic Homogenizer, 5/32″ horn) at 35 % amplitude for 5 min (14.4 kJ) to disperse. A 2 mM Cr(III) stock solution was prepared using potassium chromium(III) oxalate trihydrate ($K_3Cr(C_2O_4)_3{\cdot}3H_2O$, 98 %, Sigma Aldrich, USA). This salt was chosen to have no impact on the solution pH. [13,46,47] Bovine serum albumin (BSA, heat shock fraction, pH 7, ≥98 %, Sigma Aldrich, USA) solutions were created at 10 g/L (0.15 mM) in 150 mM NaCl and 20 mM 2-(N-morpholino)ethanesulfonic acid buffer (MES, low moisture content, ≥99 % by titration, Sigma Aldrich, USA), pH 7.2–7.4 adjusted with 8 M NaOH. The concentration of the nanoparticle suspension was chosen to optimize the colloidal stability and the volume of the aliquots added to the protein solution was chosen to emulate estimations of the amount of material released from corroding biomedical implants in vivo. [10]

2.2. Optical transmission

MES buffer solution with 10 g/L (0.15 mM) BSA was prepared and allowed to equilibrate for one hour at room temperature. 1.5 mL was transferred to a clean, dry microcentrifuge tube and centrifuged at 4000*g* for 30 s to remove any insoluble debris and dust. The top 1 mL was transferred to a clean vial containing various quantities of 50 ppm Cr_2O_3 NP suspension. The mixtures were gently stirred, and then the optical transmission was analyzed in triplicate on the Litesizer 500 (Anton Paar) over 30 s.

2.3. Zeta potential measurement

MES buffer solution with 10 g/L (0.15 mM) BSA was prepared and allowed to equilibrate for one hour at room temperature. 1.5 mL was transferred to a clean, dry microcentrifuge tube and centrifuged at 4000*g* for 30 s to remove any insoluble debris and dust. The top 1 mL was transferred to a clean vial containing various quantities of 50 ppm Cr_2O_3 NP suspension. The mixtures were gently stirred, and then a one mL aliquot was analyzed in triplicate on the Litesizer 500 (Anton Paar) in Omega Cuvettes, which can measure high-conductivity ζ potential using the cmPALS technique (continuously monitored phase analysis light scattering – which is a form of electrophoresis) after five minutes of equilibration time.

Three 1 mL aliquots of 50 ppm Cr_2O_3 nanoparticle suspension were also analyzed on the Litesizer 500 (Anton Paar) at 21 °C and with a one-minute equilibration time. In all cases, a Smoluchowski approximation was used, with a Henry factor of 1.5. Power adjustment was automatic with a maximum potential of 200.0 V. The measurement was concluded after 100 runs. The solvent was ultrapure (type 1) water (refractive index of 1.3306, a viscosity of 0.0009779 Pa × s, and a relative permittivity of 79.81).

2.4. Time of flight secondary ion mass spectrometry (ToF-SIMS)

MES buffer solution with 10 g/L (0.15 mM) BSA was prepared and equilibrated for one hour at room temperature. 1.0 mL of BSA solution and 1.0 mL of 50 ppm Cr_2O_3 nanoparticle suspension were transferred to a clean, dry 15 mL centrifuge tube and centrifuged at 4000*g* for 2 min. The top 1.5 mL was discarded, and the remaining suspension was vortex-mixed to resuspend. Metal salt solutions were made at a 24:1 M ratio of metal-to-protein. A clean Al foil was used to deposit samples with a pipette, followed by drying at room temperature overnight. The loaded Al foil was rinsed with ultrapure water for 10 s before analysis to remove excess salt. In ToF-SIMS (TOF-SIMS IV, ION-TOF GmbH, Germany), the sample surface was bombarded with a pulsed (~1 ns) 25 keV Bi_3^+ primary ion beam for the generation of ions from the surface. These secondary ions were extracted with an electric field and their times of flight in a reflectron type of tube were measured to construct a spectrum of secondary ion mass by converting the flight time to a mass/charge (m/z) ratio via known species such as hydrogen, carbon, and hydrocarbons. A low-energy electron beam was then flooded over the sample for charge compensation, which completed the 100-μs cycle of one shot of the primary ion. The base pressure of the analysis chamber of the instrument was approximately 10^{-7} mbar. The secondary ion mass spectra were collected at 128 × 128 pixels over the rastered area with one shot of pulsed primary ion beam per pixel. The ion mass spectra presented in this study were normalized to the total ion intensity and to the intensity

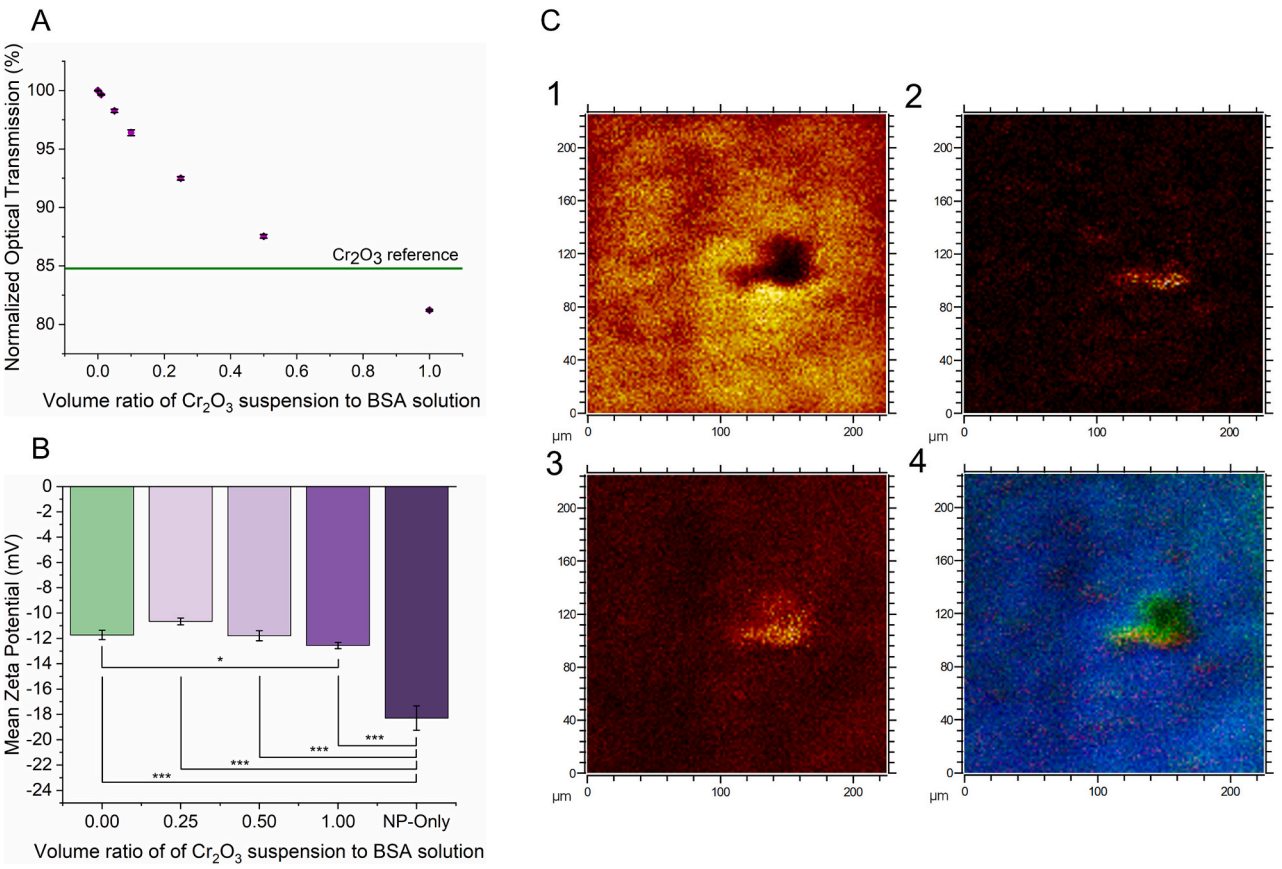

Fig. 1. Investigating the interaction of albumin with Cr_2O_3 nanoparticles: aggregation (A), protein corona (B), colocalization of proteins and nanoparticles (C). A) Optical transmission of, and B) mean zeta potential (* - $p \leq 0.05$, *** - $p \leq 0.001$) of different volume ratios of 50 ppm Cr_2O_3 nanoparticle suspension to 10 g/L BSA solution (e.g., a ratio of 1 means equal volumes of solutions) and only nanoparticle suspension. Transmission is normalized to pure BSA, with the green reference line representing the transmission of pure 50 ppm Cr_2O_3 NP suspension. C) ToF-SIMS intensity map of 1) Al^+ 2) Cr^+ 3) $C_2H_6N^+$ 4) Overlay of Al^+ (blue), Cr^+ (red), $C_2H_6N^+$ (green). All ions normalized to total ion intensity. Al signals originate from the Al foil substrate.

of ions of interest to account for concentration effects. Positive ion mass spectra were calibrated using H^+, CH_3^+, and $C_3H_5^+$. Negative ion mass spectra were calibrated using H^-, CH^-, and C_4H^-. When necessary, known, higher mass ions would be used to recalibrate the spectra. An image of an ion was obtained by mapping the intensity of the ion against the pixels. The (lateral) spatial resolution of the ion image was on the order of a few micrometres. Images selected for analysis were subdivided into 6 regions of interest of varying size and composition to increase the statistical power of the data.

2.5. Circular dichroism (CD) spectroscopy

Tris(hydroxymethane)aminomethane (20 mM, Tris, ACS reagent, ≥99.8 %, Sigma Aldrich, USA; 100 mM NaCl; pH 7.2–7.4) adjusted with 5 % HCl was used to prepare 1.0 g/L (0.015 mM) BSA samples and allowed to equilibrate for 60 min at room temperature. Tris buffer was employed for CD spectroscopy measurements instead of MES to reduce the background noise of the sample. Samples were diluted with Tris buffer or 50 ppm Cr_2O_3 nanoparticle suspension to create samples with a final protein concentration of 0.25 g/L (0.004 mM). Protein-free nanoparticle-containing blanks were created and subtracted from the protein and nanoparticle signal to eliminate the impact of nanoparticle absorption. Samples were then analyzed in triplicate between 260 and 200 nm at 37 °C on a Jasco J-810 spectropolarimeter (Easton, MD) with a 1 mm quartz cuvette.

2.6. Principal component analysis (PCA)

Principal component analysis was conducted using the Eigenvector Research, Inc. software Solo (version 9.3). Fragment ion intensity was normalized to total ion intensity within the IONTOF SurfaceLab 7.2 software, then further normalized such that each sample has a total intensity across all fragments of one to account for concentration differences. All data was “autoscaled” prior to PCA. In this procedure, the data in each column is mean-centred by subtracting the column mean from each column, forming a matrix where each column has a mean of zero. Each mean-centred variable is then divided by its standard deviation, which results in variables with unit variance. This procedure puts all variables on an equal basis for analysis. No cross-validation methods were applied, and the first two principal components were selected to investigate the clustering tendency of scores for different samples.

2.7. Statistical analysis

To determine if the differences between two sets of data of similar type is statistically significant, an unpaired two-tailed Student's *t*-test was used. This is a statistical hypothesis test that follows a Student's t-distribution under the null hypothesis. If the probability (p) that these sets of data were equal was smaller than 0.05, then they were considered statistically different.

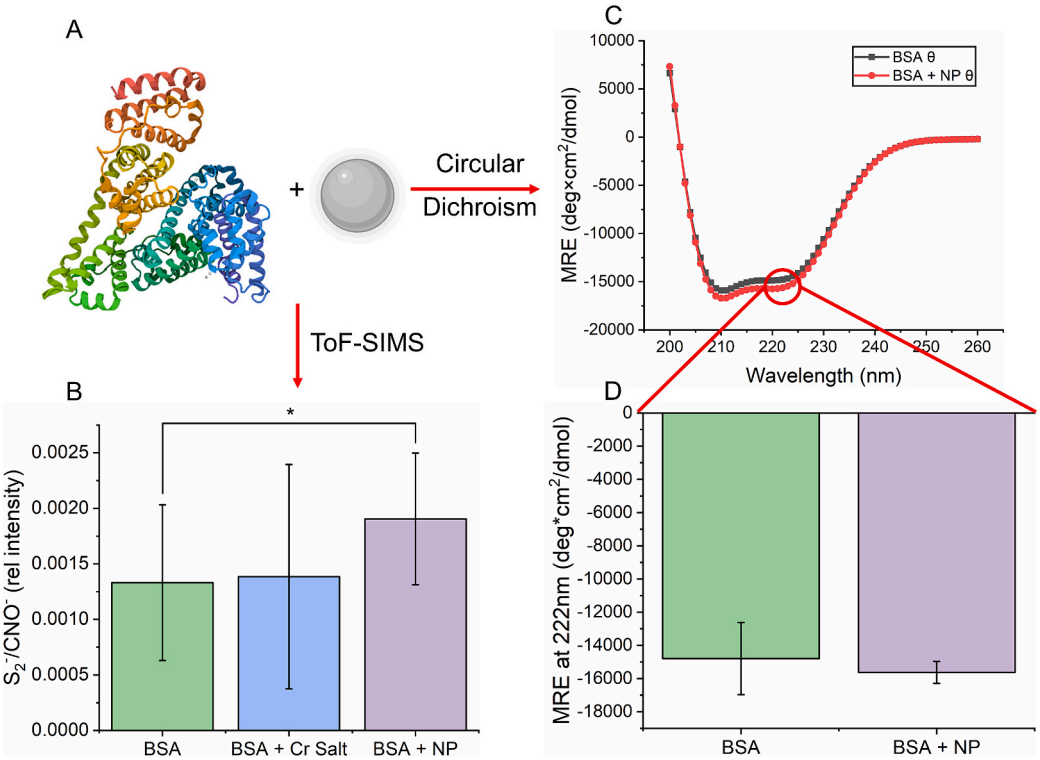

Fig. 2. Investigating the unfolding of albumin in the presence of Cr_2O_3 nanoparticles, schematically represented in A), by B) disulfide signal per CNO^- by ToF-SIMS (* - $p \leq 0.05$), C) Far UV scan of BSA and BSA + 0.25 mL Cr_2O_3 nanoparticle suspension, and D) a comparison of the CD ellipticity measured at 222 nm ($p = 0.2794$).

3. Results and discussion

3.1. Interaction of Cr_2O_3 nanoparticles with BSA

The addition of suspended insoluble material, such as Cr_2O_3 nanoparticles, to a solution will naturally reduce the optical transmission as the turbidity increases. Normalizing all values to the transmission of a pure solution of BSA, the addition of various quantities of Cr_2O_3 suspension resulted in a reduction of the optical transmission of the mixture, as seen in Fig. 1A. The turbidity in the mixture exceeds the value seen in a pure suspension of nanoparticles ($p < 0.001$), suggesting that the nanoparticles are in some way interacting with the proteins and causing aggregation. Zeta potential analysis revealed that adding Cr_2O_3 nanoparticles yielded a mean zeta potential similar to pure BSA suggesting the formation of a protein corona. The average zeta potential of BSA was -11.73 ± 0.38 mV, while the average zeta potential of the nanoparticle suspension was -18.29 ± 0.96 mV ($p < 0.001$) as seen in Fig. 1B. Adding 0.25 mL of 50 ppm Cr_2O_3 suspension to 1.0 mL of 10 g/L BSA yielded a zeta potential of -10.66 ± 0.27 mV, while 0.5 mL of Cr_2O_3 yielded a zeta potential of -11.79 ± 0.40 mV, and 1.0 mL of Cr_2O_3 yielded a zeta potential of -12.56 ± 0.25 mV. These values significantly differ compared to the BSA-free nanoparticle suspension's measured value ($p < 0.001$ in all cases). The dramatic reduction of the nanoparticle zeta potential in the presence of BSA suggests that BSA is adsorbing to the surface of the nanoparticles, altering the surface charge of the nanoparticle, which is why the measured zeta potential is so similar to that of pure BSA.

The imaging capabilities of ToF-SIMS make it ideal for the visualization of complex systems like the protein coronas of nanoparticles. ToF-SIMS intensity maps provide detailed images of sample surfaces and may be employed to visualize colocalization between protein material and nanoparticle (Fig. 1C). The fragment $C_2H_6N^+$ is a prevalent ion arising from proteinaceous materials. [48–51] Fig. 1C shows representative ion images of the colocalization of the Cr^+ (Fig. 1C_2) and proteinaceous (Fig. 1C_3) fragments (and the corresponding absence of substrate signals in Fig. 1C_1). This finding was reproducible across several ion images, suggesting a preferential interaction of proteins with Cr_2O_3 nanoparticles.

We have carefully inspected both the positive and negative secondary ion mass spectra but did not find any ion fragment containing Cr and N or C. Therefore, there is no direct evidence from the ToF-SIMS data to specify the binding site of the protein on the Cr_2O_3 nanoparticles, which may be regarded as the weakness of the technique. However, due to the detection of numerous ion fragments in ToF-SIMS data, one can extract information hidden in those ion fragments by exploring the relationships among the ion fragments, which will be discussed later.

3.2. Protein unfolding

Circular dichroism was employed to determine if the addition of Cr_2O_3 nanoparticles resulted in the unfolding of BSA. The far UV scan of pure BSA and BSA with 0.25 mL of 50 ppm Cr_2O_3 nanoparticle suspension is seen in Fig. 2C., while a comparison of the CD signal at 222 nm is found in Fig. 2D. Previous studies have indicated that the addition of $K_3Cr(C_2O_4)_3{\cdot}3H_2O$ chromium salt did not result in any protein unfolding by circular dichroism. [13] Likewise, there was no significant difference between the scan of BSA and the scan of BSA with Cr_2O_3 nanoparticles, suggesting that the addition of nanoparticles at the concentration of this study did not result in protein unfolding. This is the expected result, as Cr_2O_3 nanoparticles are an order of magnitude larger than BSA and have a large radius of curvature. Further investigation into the unfolding was carried out using ToF-SIMS in negative ion mode, using the ratio of S_2^- (disulfide bond) to CNO^- (peptide bond) fragments (Fig. 2B). This method has been used previously to investigate protein denaturation and is highly effective due to the shallow depth profile of ToF-SIMS, and the relatively large size of BSA in comparison. [41,52–54]

It was determined that the interaction of BSA with Cr(III) ions did not result in the reduction or cleavage of the cystine bridges, with a S_2^-/CNO^- ratio of $1.33 \pm 0.70 \times 10^{-3}$ and $1.39 \pm 1.0 \times 10^{-3}$ for BSA and

Table 1
Selected positive ToF-SIMS fragments and their corresponding amino acids.

Mass (*m/z*)	Fragment	Corresponding amino acid	Amino acid charge	Ref(s)
30.03	CH_4N^+	Gly, Lys, Leu, others	0	[48–51]
44.05	$C_2H_6N^+$	Ala, others	0	[48–51]
58.07	$C_3H_8N^+$	Glu	(−)	[49]
59.05	$CH_5N_3^+$	Arg	(+)	[49–51]
70.03	$C_3H_4NO^+$	Asn, Asp	0/(−)	[48–51]
70.07	$C_4H_8N^+$	Pro, Arg, Val, Leu	0	[48,49,51]
72.08	$C_4H_{10}N^+$	Val	0	[49–51]
73.06	$C_2H_7N_3^+$	Arg	(+)	[48,49,51]
74.06	$C_3H_8NO^+$	Thr	0	[48–51]
76.02	$C_2H_6NS^+$	Cys	0	[50]
81.04	$C_4H_5N_2^+$	His	0	[48,50,51]
84.04	$C_4H_6NO^+$	Gln, Glu	0/(−)	[48–51]
84.08	$C_5H_{10}N^+$	Lys	(+)	[48–51]
91.05	$C_7H_7^+$	Phe	0	[51]
100.08	$C_4H_{10}N_3^+$	Arg	(+)	[48–51]
107.05	$C_7H_7O^+$	Tyr	0	[48–51]
110.07	$C_5H_8N_3^+$	His, Arg	0/(+)	[48,49,51]
120.08	$C_8H_{10}N^+$	Phe	0	[48–51]
130.06	$C_9H_8N^+$	Trp	0	[48–51]
136.08	$C_8H_{10}NO^+$	Tyr	0	[48,51]

BSA + Cr(III), respectively ($p = 0.43$). This suggests that Cr(III) does not result in any protein unfolding, as this rigid bonding motif prevents molecular flexibility and is a key factor that determines protein tertiary structure. [52,55] This is consistent with our previous work, which showed that the addition of Cr(III) ions to a BSA solution did not result in any global protein unfolding. [13] When exposed to Cr_2O_3 nanoparticles, the relative intensity of the disulfide fragment increased from $1.33 \pm 0.70 \times 10^{-3}$ to $1.91 \pm 0.59 \times 10^{-3}$ ($p = 0.020$).

The observed increase in disulfide fragment intensity must be due to conformational changes within the protein. Native BSA contains 17 intrachain disulfide bonds and only one free cysteine with a reduced sulfhydryl group. This eliminates the possibility of forming new cystine linkages through redox reactions, meaning the observed increase in fragment intensity must arise from a conformational change. [55] Circular dichroism data does not indicate any loss of conformation or unfolding, so we suggest that the relative increase in disulfide intensity was due to the orientation of BSA molecules bound to the nanoparticle surface. The preferential interaction between protein and nanoparticle may result in uniform or semi-uniform orientation of BSA molecules on the nanoparticle surface, which, when compared to the random molecular orientation in drop-cast BSA and BSA + Cr(III) salt samples, may uniformly expose a face of the protein richer in oxidized disulfide linkages, yielding a greater measured intensity by ToF-SIMS.

3.3. Principal component analysis (PCA)

The complete list of fragments and their associated amino acids used in the PCA analysis can be found in Table 1 below. In some instances, no viable amino acid fragments could be found for surface-abundant amino acids, specifically aspartic acid or serine. This was due to poor peak resolution, interference with neighbouring peaks, or the complete absence of the peak due to low relative fragment abundance. The PCA result accounted for a larger portion of sample trends for the BSA + Cr_2O_3 nanoparticle samples than the BSA + Cr(III) salt samples, however in both cases, >75 % of the sample data can be explained by the first two PCs. The sample scores can be seen in Table S1 and Fig. S5 in the Supporting Information.

The variable statistics for the BSA + NP are presented in Fig. 3A. The fragments most closely associated with the chromium fragment Cr^+ in the PCA result (smallest distance to Cr^+ in Fig. 3B, high covariance) are seen in Fig. 3B. In all cases there is a positive correlation between the detected intensity of these protein fragments and the chromium fragment, meaning that the protein fragments increased in intensity in the presence of the chromium fragment associated with the Cr_2O_3 nanoparticles (Fig. 3A).

This measured increase in intensity may only be attributed to the spatial orientation of BSA within the system, as the increase can't be linked to any changes in the concentration of the individual amino acids or unfolding. This change must instead be due to the orientation of BSA on the nanoparticle surface. The PCA result suggests that the fragments most closely associated with Cr^+ are those from either neutral or negative amino acids. The intensity of fragments associated with positive amino acids decreases in most cases, as seen in Fig. 4B.

The measured zeta potential of the Cr_2O_3 nanoparticles was −18.29 ± 0.96 mV. The decrease in positive ion intensity in ToF-SIMS may be attributed to the electrostatic interaction between positively charged amino acids and the negatively charged surface of the Cr_2O_3 nanoparticle, resulting in a preferential orientation of BSA on the nanoparticle surface. This would reduce the measured intensity of those fragments most abundant at the protein-nanoparticle interface due to ToF-SIMS' shallow probing depth, and artificially increase the intensity of those fragments on the opposite face of the nanoparticle - those likely least involved in the binding to the nanoparticle surface, accounting for their positive correlation with the Cr^+ ion.

In comparison, the variable statistics for the BSA + Cr(III) salt are less polarized, and the change in detected fragment intensity between BSA and BSA + Cr(III) is much smaller than for BSA and BSA + Cr_2O_3 nanoparticles. This is expected since drop-cast samples of BSA and BSA with Cr(III) should not have a preferential alignment and should,

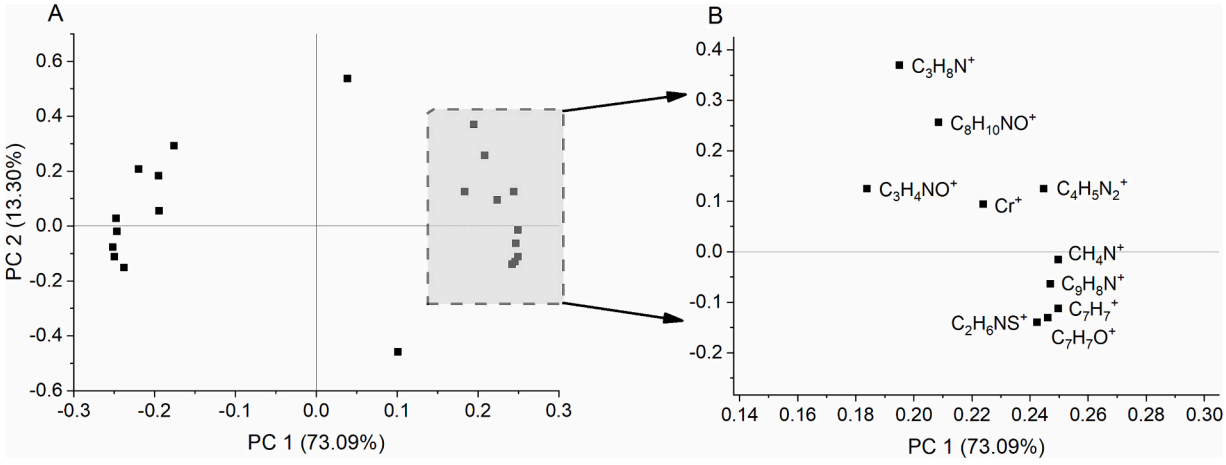

Fig. 3. Variable statistics for BSA and BSA + NP. A) Scores for all variables, an enlarged plot of the grey rectangle is seen in B) for the fragments with the shortest distance to Cr^+ in the principal component matrix.

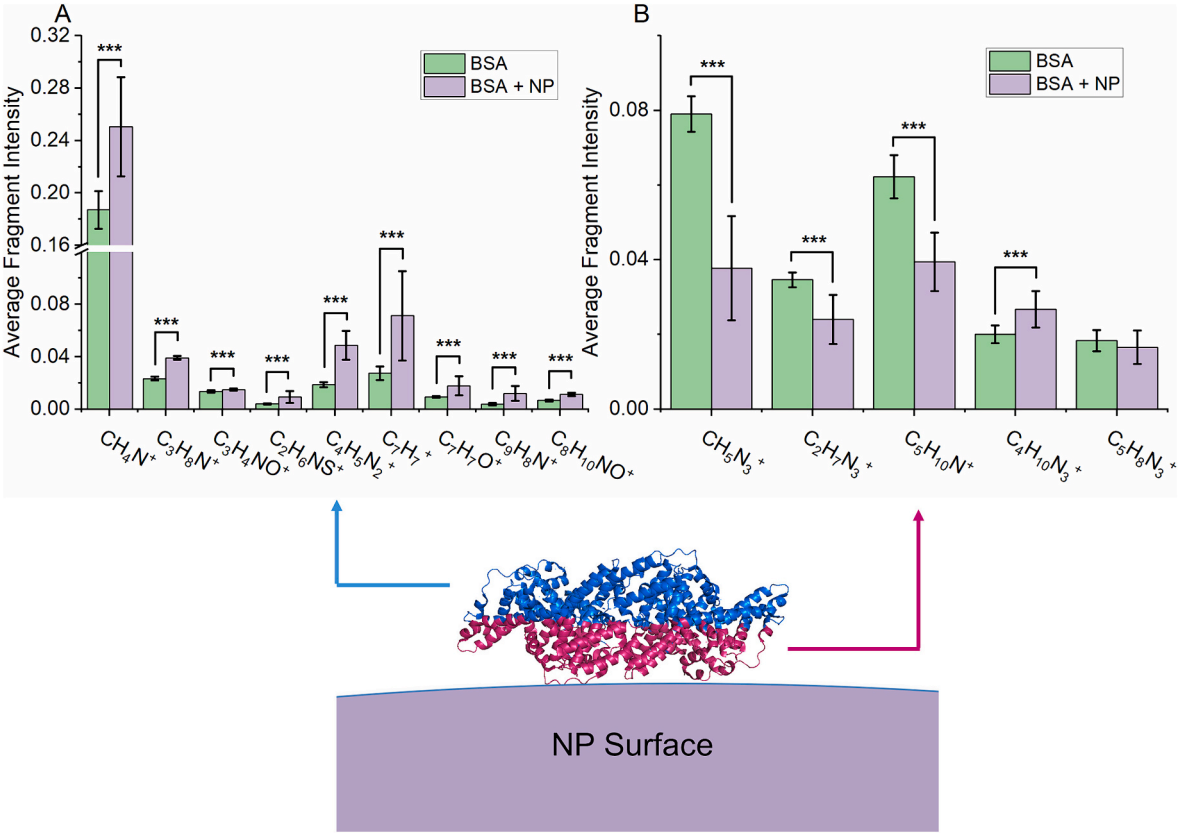

Fig. 4. Detected intensities of fragments A) from neutral and negative amino acids associated with Cr^+ fragment by PCA result, B) associated with positive amino acids (*** - $p \leq 0.001$).

therefore, be heterogeneously oriented on the substrate surface. Additionally, a close correlation was found between the Cr^+ ions and fragments arising from glutamic and aspartic acids and asparagine, suggesting a salt-bridging mechanism of interaction between the positively charged Cr(III) cation (after dissociation from the oxalate anion) and negatively charged acid residues. A full investigation of the Cr(III)-BSA interaction and the proposed mechanism can be found in section S4 of the Supporting Information.

3.4. Proposed mechanism

PCA results indicate that when exposed to Cr_2O_3 nanoparticles, the amino acids most associated with the chromium ion are negative and neutral, and the detected intensity of these fragments increases, while the intensity of all positively charged amino acid fragments decreases. ToF-SIMS is a highly surface-sensitive technique (1–3 nm, with the strongest signal from the first 1 nm), which suggests that the positively charged amino acids were being sequestered away from the protein-vacuum interface. The surface charge of the Cr_2O_3 nanoparticles was found to be negative under our physiologically relevant testing conditions. We propose that BSA will preferentially orient on the nanoparticle surface such that a surface rich in positive amino acids interacts with the negative metal oxide surface, explaining the reduction in their detected intensity. Amino acids populating the surface of the protein facing outwards were detected in greater intensity, including disulfide linkages, resulting in the measured increase in S_2^-/CNO^- ratio.

The proposed mechanism is valid for the conditions studied: physiological pH, ionic strength, and unfunctionalized Cr_2O_3 nanoparticles of <100 nm diameter. Although this is representative of the average size of released wear nanoparticles from biomedical implants, extremely small particles may be released *in vivo*. [10,56] These extremely small particles (< 50 nm) might interact differently with albumin and perhaps result in protein unfolding due to their smaller radius of curvature. The techniques used to study protein unfolding in this work broadly assess global protein structure; it is possible that at the protein-nanoparticle interface, there is a localized breakdown of protein secondary or tertiary structure not detected by our methods. Additionally, the complex nature of biological environments may also impact the kinetics of this process, as different macromolecules will possess different affinities for the nanoparticle surface. The isoelectric point of serum proteins is suspected to have a large influence on their binding to these nanoparticles, and proteins with a higher pI, which will carry a greater positive charge at physiological pH, such as hemoglobin and lysozyme are expected to have a greater affinity for Cr_2O_3 nanoparticles than albumin. [57] Likewise, the size of the proteins might influence their surface affinity and kinetics of adsorption and/or exchange of already adsorbed proteins (Vroman effect). [58]

3.5. Computational verification

An explicit all-atom molecular dynamics simulation was ruled outside the scope of this work due to a lack of parameterization in existing force fields for the strength of the protein-surface interactions. However, it is possible to perform a coarse-grained simulation of BSA using a non-linear Poisson Boltzmann formalism, specifically the Adaptive Poisson-Boltzmann Solver (APBS release 3.4.1) paired with PDB2PQR. [59] The web tool PDB2PQR was used to prepare structural data and force field parameters for the crystal structure of BSA (PDB code 3V03 from https://www.rcsb.org/). This data was then fed into APBS to solve the equations of continuum electrostatics. Visualization was carried out using PyMol (version 2.5.4).

BSA has an isoelectric point between 5.0 and 5.6 pH units, meaning it carries a net negative charge at physiological pH. [60] Regardless, Fig. 5 shows that BSA has a solvent-accessible region of predominantly

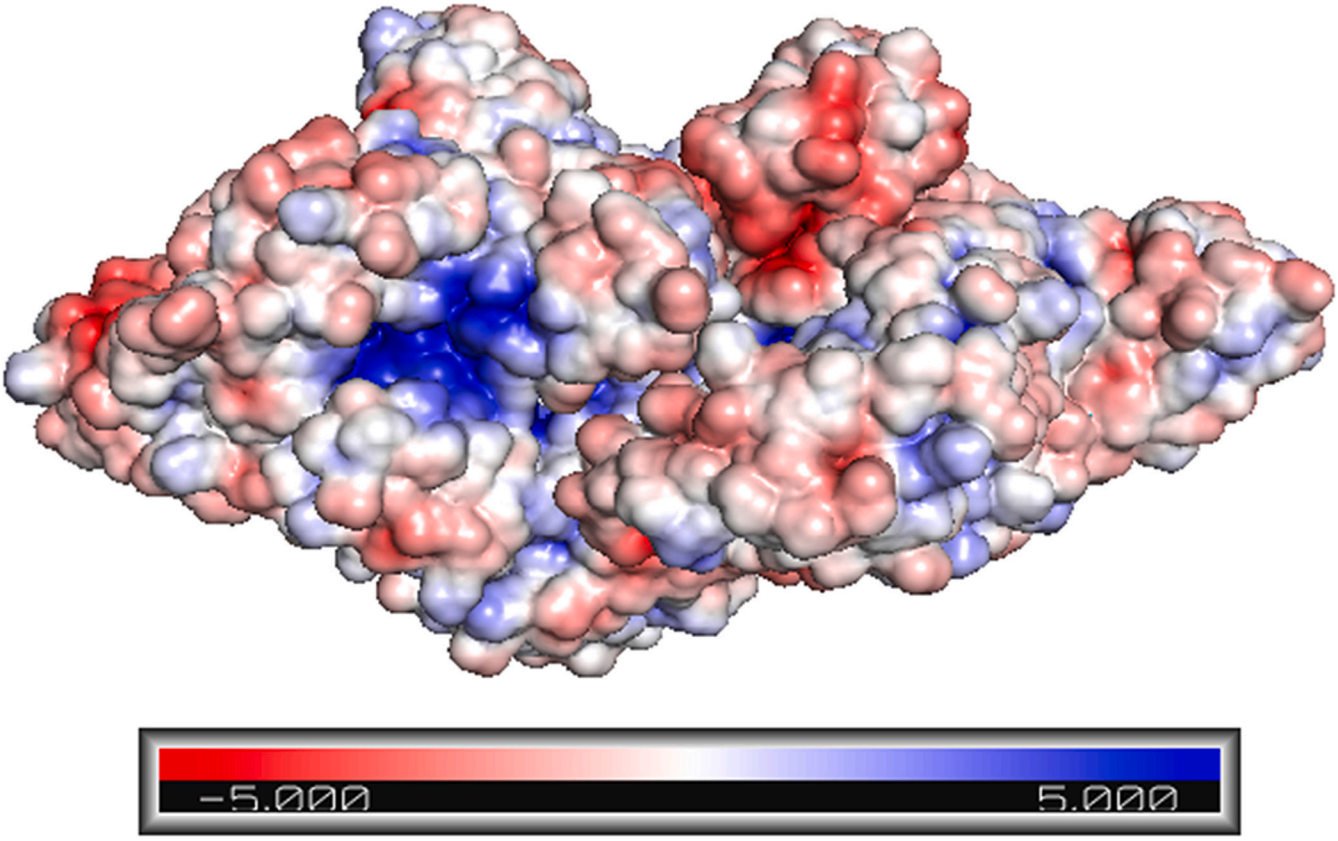

Fig. 5. Solvent-accessible map of APBS electrostatics of BSA. Generated from the PDB file 3 V03 using PDB2PQR, APBS, and PyMol for visualization.

positive charge, supporting our proposed interaction mechanism between BSA and Cr_2O_3 nanoparticles.

4. Conclusions

This study used CD spectroscopy, electrophoretic mobility, and ToF-SIMS to investigate the binding of BSA to Cr(III) and Cr_2O_3 nanoparticles in physiological conditions. It was determined that neither chromium species resulted in global protein unfolding under the conditions investigated. This work demonstrates there is a strong degree of interaction between negatively charged amino acid residues and Cr(III) ions, substantiating the claim that Cr(III)-induced protein aggregation proceeds via a salt-bridging mechanism. This work proves there is a preferential interaction between positively charged amino acid residues with the Cr_2O_3 nanoparticle surface. This confirms our hypothesis that neither Cr(III) ions nor chromium oxide nanoparticles result in global protein unfolding, however, both metal species interact strongly with albumin and may be implicated in the formation of Cr-albumin aggregates. These fundamental research findings will help improve the study of metal ions and metal nanoparticles in proteinaceous environments and help improve our understanding of the potential risks of biomedical implant corrosion and nanomedicine.

CRediT authorship contribution statement

Zoltan Wolfgang Richter-Bisson: Writing – original draft, Visualization, Validation, Supervision, Methodology, Investigation, Funding acquisition, Formal analysis, Conceptualization. **Heng-Yong Nie:** Writing – review & editing, Visualization, Validation, Methodology, Conceptualization. **Yolanda Susanne Hedberg:** Writing – review & editing, Visualization, Supervision, Resources, Project administration, Methodology, Funding acquisition, Conceptualization.

Declaration of competing interest

The authors declare the following financial interests/personal relationships which may be considered as potential competing interests: Zoltan Richter-Bisson reports financial support was provided by Ontario Ministry of Colleges and Universities. Yolanda Hedberg reports financial support was provided by Ontario Ministry of Colleges and Universities. Yolanda Hedberg reports financial support was provided by Canada Foundation for Innovation. Yolanda Hedberg reports financial support was provided by Natural Sciences and Engineering Research Council of Canada. Yolanda Hedberg reports financial support was provided by Canada Research Chairs Program. If there are other authors, they declare that they have no known competing financial interests or personal relationships that could have appeared to influence the work reported in this paper.

Data availability statement

Raw data is available on the platform Open Science Framework (https://osf.io/8yjpt/?view_only=b4d0af385ebb47fc92dba310e58f89e9).

Acknowledgements

Daria Baskova is acknowledged for her artistic assistance with the graphical abstract. Yolanda Hedberg reports financial support was provided by the Ontario Ministry of Colleges and Universities, Ontario Research Fund (Early Researcher Award [ER22-17-268], Small Infrastructure Fund [42507]), the Canada Foundation for Innovation (John R. Evans Leaders Fund [42507]), the Natural Sciences and Engineering Research Council of Canada (Discovery Grants - DND Supplement [DGDND-2021-03997], Discovery Grants [RGPIN-2021-03997]), the Canada Research Chairs Program (Tier 2 [CRC-2019-00425]), and the

University of Western Ontario (Wolfe-Western Fellowship [2020], startup funds [Chemistry 2020]). Zoltan Richter-Bisson reports financial support was provided by the Ontario Ministry of Colleges and Universities (QEII OGS).

Appendix A. Supplementary data

Supplementary data to this article can be found online at https://doi.org/10.1016/j.ijbiomac.2024.134845.

References

[1] J.A. Singh, Epidemiology of Knee and Hip Arthroplasty: A Systematic Review. The, Open Orthop. J. 5 (1) (2011) 80–85, https://doi.org/10.2174/1874325001105010080.
[2] C. Pabinger, A. Geissler, Utilization rates of hip arthroplasty in OECD countries, Osteoarthr. Cartil. 22 (2014) 734–741, https://doi.org/10.1016/j.joca.2014.04.009.
[3] Healthcare Market Research Report, 2024.
[4] Y.S. Hedberg, I. Odnevall Wallinder, Metal release from stainless steel in biological environments: a review, Biointerphases 11 (2016) 018901, https://doi.org/10.1116/1.4934628.
[5] N.S. Manam, W.S.W. Harun, D.N.A. Shri, S.A.C. Ghani, T. Kurniawan, M.H. Ismail, M.H.I. Ibrahim, Study of corrosion in biocompatible metals for implants: a review, J. Alloys Compd. 701 (2017) 698–715, https://doi.org/10.1016/j.jallcom.2017.01.196.
[6] G. Manivasagam, D. Dhinasekaran, A. Rajamanickam, Biomedical Implants: Corrosion and its Prevention-A Review 2 (2010) 40–54, https://doi.org/10.2174/1877610801002010040.
[7] J. Rituerto Sin, X. Hu, N. Emami, Tribology, corrosion and tribocorrosion of metal on metal implants, tribology - materials, Surfaces and Interfaces 7 (2013) 1–12, https://doi.org/10.1179/1751584X13Y.0000000022.
[8] Z. Zhou, Q. Shi, J. Wang, X. Chen, Y. Hao, Y. Zhang, X. Wang, The unfavorable role of titanium particles released from dental implants, Nanotheranostics 5 (2021) 321–332, https://doi.org/10.7150/ntno.56401.
[9] H. Matusiewicz, Potential release of in vivo trace metals from metallic medical implants in the human body: from ions to nanoparticles - a systematic analytical review, Acta Biomater. 10 (2014) 2379–2403, https://doi.org/10.1016/j.actbio.2014.02.027.
[10] A.K. Madl, M. Liong, M. Kovochich, B.L. Finley, D.J. Paustenbach, G. Oberdörster, Toxicology of wear particles of cobalt-chromium alloy metal-on-metal hip implants part I: physicochemical properties in patient and simulator studies, Nanomedicine 11 (2015) 1201–1215, https://doi.org/10.1016/j.nano.2014.12.005.
[11] X. Qi, Y. Li, M. Shen, Q. Yu, Y. Chen, J. Xie, Formation of rice protein fibrils is highly sensitive to the different types of metal ions: aggregation behavior and possible mechanisms, Food Chem. 431 (2024), https://doi.org/10.1016/j.foodchem.2023.137101.
[12] A.C. Kim, S. Lim, Y.K. Kim, Metal ion effects on Aβ and tau aggregation, Int. J. Mol. Sci. 19 (2018), https://doi.org/10.3390/ijms19010128.
[13] Z.W. Richter-Bisson, A. Doktor, Y.S. Hedberg, Serum albumin aggregation facilitated by cobalt and chromium metal ions, ACS Appl. Bio Mater. 6 (2023) 3832–3841, https://doi.org/10.1021/acsabm.3c00463.
[14] S.J. Park, Protein–nanoparticle interaction: Corona formation and conformational changes in proteins on nanoparticles, Int. J. Nanomedicine 15 (2020) 5783–5802, https://doi.org/10.2147/IJN.S254808.
[15] M. Schäffler, M. Semmler-Behnke, H. Sarioglu, S. Takenaka, A. Wenk, C. Schleh, S. M. Hauck, B.D. Johnston, W.G. Kreyling, Serum protein identification and quantification of the corona of 5, 15 and 80 nm gold nanoparticles, Nanotechnology 24 (2013), https://doi.org/10.1088/0957-4484/24/26/265103.
[16] H.J. Münch, S.S. Jacobsen, J.T. Olesen, T. Menné, K. Soballe, J.D. Johansen, J. P. Thyssen, The association between metal allergy, total knee arthroplasty, and revision, Acta Orthop. 86 (2015) 378–383, https://doi.org/10.3109/17453674.2014.999614.
[17] H. Pandit, S. Glyn-Jones, P. Mclardy-Smith, R. Gundle, D. Whitwell, C.L. M. Gibbons, S. Ostlere, N. Athanasou, H.S. Gill, D.W. Murray, Pseudotumours associated with metal-on-metal hip resurfacings, J. Bone Joint Surg. Br. 90 (2008) 847–851, https://doi.org/10.1302/0301-620X.90B7.
[18] P. Wagner, H. Olsson, L. Lidgren, O. Robertsson, J. Ranstam, Increased cancer risks among arthroplasty patients: 30 year follow-up of the Swedish knee arthroplasty register, Eur. J. Cancer 47 (2011) 1061–1071, https://doi.org/10.1016/j.ejca.2010.11.023.
[19] R. Rajan, S. Ahmed, N. Sharma, N. Kumar, A. Debas, K. Matsumura, Review of the current state of protein aggregation inhibition from a materials chemistry perspective: special focus on polymeric materials, Mater Adv 2 (2021) 1139–1176, https://doi.org/10.1039/d0ma00760a.
[20] S. Lee, M.C. Choi, K. Al Adem, S. Lukman, T.Y. Kim, Aggregation and cellular toxicity of pathogenic or non-pathogenic proteins, Sci. Rep. 10 (2020), https://doi.org/10.1038/s41598-020-62062-3.
[21] B.G. Poulson, K. Szczepski, J.I. Lachowicz, L. Jaremko, A.H. Emwas, M. Jaremko, Aggregation of biologically important peptides and proteins: inhibition or acceleration depending on protein and metal ion concentrations, RSC Adv. 10 (2019) 215–227, https://doi.org/10.1039/c9ra09350h.
[22] F. Di Spirito, R. Lo Giudice, M. Amato, M.P. Di Palo, F. D'Ambrosio, A. Amato, S. Martina, Inflammatory, reactive, and hypersensitivity lesions potentially due to metal nanoparticles from dental implants and supported restorations, An Umbrella Review, Applied Sciences (Switzerland) 12 (2022), https://doi.org/10.3390/app122111208.
[23] E.A. Kumah, R.D. Fopa, S. Harati, P. Boadu, F.V. Zohoori, T. Pak, Human and environmental impacts of nanoparticles: a scoping review of the current literature, BMC Public Health 23 (2023), https://doi.org/10.1186/s12889-023-15958-4.
[24] C.M. Duarte, L. Jaremko, M. Jaremko, Hypothesis: potentially systemic impacts of elevated CO2 on the human proteome and health, Front. Public Health 8 (2020), https://doi.org/10.3389/FPUBH.2020.543322/FULL.
[25] S. Tran, P. DeGiovanni, B. Piel, P. Rai, Cancer nanomedicine: a review of recent success in drug delivery, Clin. Transl. Med. 6 (2017), https://doi.org/10.1186/s40169-017-0175-0.
[26] M.G. Mokwena, C.A. Kruger, M.T. Ivan, A. Heidi, A review of nanoparticle photosensitizer drug delivery uptake systems for photodynamic treatment of lung cancer, Photodiagnosis Photodyn. Ther. 22 (2018) 147–154, https://doi.org/10.1016/j.pdpdt.2018.03.006.
[27] P.-J. Cunat, Alloying Elements in Stainless Steel and Other Chromium-Containing Alloys. www.euroinox.org, 2004. (Accessed 19 May 2023).
[28] A. Hartmann, F. Hannemann, J. Lützner, A. Seidler, H. Drexler, K.-P. Günther, J. Schmitt, Metal ion concentrations in body fluids after implantation of hip replacements with metal-on-metal bearing – systematic review of clinical and epidemiological studies, PloS One 8 (2013) e70359, https://doi.org/10.1371/journal.pone.0070359.
[29] T. Topală, A. Bodoki, L. Oprean, R. Oprean, Bovine serum albumin interactions with metal complexes, Clujul Medical 87 (2014) 215–219, https://doi.org/10.15386/cjmed-357.
[30] H. M, E. Azzazy, R.H. Christenson, All about albumin: biochemistry, genetics, and medical applications., Clin. Chem. 43 (1997) 2014a–22015. doi:https://doi.org/10.1093/clinchem/43.10.2014a.
[31] S.K. Ghosh, D. Choudhury, N. Das, B. Pingguan-Murphy, Tribological role of synovial fluid compositions on artificial joints — a systematic review of the last 10 years, Lubr. Sci. 26 (2014) 387–410, https://doi.org/10.1002/ls.1266.
[32] K.M.N. Oates, W.E. Krause, R.L. Jones, R.H. Colby, Rheopexy of synovial fluid and protein aggregation, J. R. Soc. Interface 3 (2006) 167–174, https://doi.org/10.1098/rsif.2005.0086.
[33] M. Aleksić, C.K.S. Pease, D.A. Basketter, M. Panico, H.R. Morris, A. Dell, Investigating protein haptenation mechanisms of skin sensitisers using human serum albumin as a model protein, Toxicol. In Vitro 21 (4) (2007) 723–733, https://doi.org/10.1016/J.TIV.2007.01.008.
[34] A. Benninghoven, Chemical analysis of inorganic and organic surfaces and thin films by static time-of-flight secondary ion mass spectrometry (TOF-SIMS), Angew. Chem. Int. Ed. Engl. 33 (1994) 1023–1043, https://doi.org/10.1002/anie.199410231.
[35] S. Muramoto, G. Gillen, E.S. Windsor, Chemical discrimination of multilayered paint cross sections for potential forensic applications using time-of-flight secondary ion mass spectrometry, Surf. Interface Anal. 50 (2018) 889–896, https://doi.org/10.1002/sia.6509.
[36] H.-Y. Nie, Self-assembled monolayers of octadecylphosphonic acid and polymer films: surface chemistry and chemical structures studied by time-of-flight secondary ion mass spectrometry, Surf. Interface Anal. 49 (2017) 1431–1441, https://doi.org/10.1002/sia.6296.
[37] N. Xia, C.J. May, S.L. McArthur, D.G. Castner, Time-of-flight secondary ion mass spectrometry analysis of conformational changes in adsorbed protein films, Langmuir 18 (2002) 4090–4097, https://doi.org/10.1021/la020022u.
[38] S. Muramoto, D.J. Graham, M.S. Wagner, T. Geol Lee, D. Won Moon, D.G. Castner, ToF-SIMS analysis of adsorbed proteins: principal component analysis of the primary ion species effect on the protein fragmentation patterns, J. Phys. Chem. C 115 (2011) 24247–24255, https://doi.org/10.1021/jp208035x.
[39] M. Henry, C. Dupont-Gillain, P. Bertrand, Conformation change of albumin adsorbed on polycarbonate membranes as revealed by ToF-SIMS, Langmuir 19 (2003) 6271–6276, https://doi.org/10.1021/la034081z.
[40] R.N. Foster, E.T. Harrison, D.G. Castner, ToF-SIMS and XPS characterization of protein films adsorbed onto bare and sodium Styrenesulfonate-grafted gold substrates, Langmuir 32 (2016) 3207–3216, https://doi.org/10.1021/acs.langmuir.5b04743.
[41] Y.S. Hedberg, M.S. Killian, E. Blomberg, S. Virtanen, P. Schmuki, I. Odnevall Wallinder, Interaction of bovine serum albumin and lysozyme with stainless steel studied by time-of-flight secondary ion mass spectrometry and X-ray photoelectron spectroscopy, Langmuir 28 (2012) 16306–16317, https://doi.org/10.1021/la3039279.
[42] I.M. Kempson, A.L. Martin, J.A. Denman, P.W. French, C.A. Prestidge, T.J. Barnes, Detecting the presence of denatured human serum albumin in an adsorbed protein monolayer using TOF−SIMS, Langmuir 26 (2010) 12075–12080, https://doi.org/10.1021/la101253g.
[43] N.G. Welch, R.M.T. Madiona, J.A. Scoble, B.W. Muir, P.J. Pigram, ToF-SIMS and principal component analysis investigation of denatured, surface-adsorbed antibodies, Langmuir 32 (2016) 10824–10834, https://doi.org/10.1021/acs.langmuir.6b02754.
[44] M. Greenacre, P.J.F. Groenen, T. Hastie, A.I. D'Enza, A. Markos, E. Tuzhilina, Principal component analysis, Nature Reviews Methods Primers 2 (2022) 100, https://doi.org/10.1038/s43586-022-00184-w.
[45] H. Abdi, L.J. Williams, Principal component analysis 2 (2010) 433–459, https://doi.org/10.1002/wics.101.

[46] A.K. Verma, R. Kore, D.R. Corbin, M.B. Shiflett, Metal recovery using oxalate chemistry: a technical review, Ind. Eng. Chem. Res. (2019), https://doi.org/10.1021/ACS.IECR.9B02598.
[47] Y.S. Hedberg, B. Erfani, M. Matura, C. Lidén, Chromium(III) release from chromium-tanned leather elicits allergic contact dermatitis: a use test study, Contact Dermatitis 78 (2018) 307–314.
[48] J.B. Lhoest, M.S. Wagner, C.D. Tidwell, D.G. Castner, Characterization of adsorbed protein films by time of flight secondary ion mass spectrometry, J. Biomed. Mater. Res. 57 (2001) 432–440, https://doi.org/10.1002/1097-4636(20011205)57:3<432::AID-JBM1186>3.0.CO;2-G.
[49] M. Henry, P. Bertrand, Surface composition of insulin and albumin adsorbed on polymer substrates as revealed by multivariate analysis of ToF-SIMS data, Surf. Interface Anal. 41 (2009) 105–113, https://doi.org/10.1002/sia.2993.
[50] X. Cheng, H.E. Canavan, D.J. Graham, D.G. Castner, B.D. Ratner, Temperature dependent activity and structure of adsorbed proteins on plasma polymerized N-isopropyl acrylamide, Biointerphases 1 (2006) 61–72, https://doi.org/10.1116/1.2187980.
[51] J. Wald, C. Müller, M. Wahl, W. Hoth-Hannig, M. Hannig, M. Kopnarski, C. Ziegler, ToF-SIMS investigations of adsorbed proteins on dental titanium, Physica status solidi (a) applications and materials, Science 207 (2010) 831–836, https://doi.org/10.1002/pssa.200983308.
[52] M.S. Killian, H.M. Krebs, P. Schmuki, Protein denaturation detected by time-of-flight secondary ion mass spectrometry, Langmuir 27 (2011) 7510–7515, https://doi.org/10.1021/la200704s.
[53] D.G. Castner, B.D. Ratner, Biomedical surface science: foundations to frontiers, Surf. Sci. 500 (2002) 28–60, https://doi.org/10.1016/S0039-6028(01)01587-4.
[54] T. Mouhib, A. Delcorte, C. Poleunis, M. Henry, P. Bertrand, C60 SIMS depth profiling of bovine serum albumin protein-coating films: a conformational study, Surf. Interface Anal. 42 (2010) 641–644, https://doi.org/10.1002/sia.3349.
[55] Y.N. Kang, H. Kim, W.S. Shin, G. Woo, T.W. Moon, Effect of disulfide bond reduction on bovine serum albumin-stabilized emulsion gel formed by microbial transglutaminase, J. Food Sci. 68 (2003) 2215–2220, https://doi.org/10.1111/j.1365-2621.2003.tb05749.x.
[56] H. Matusiewicz, M. Richter, Potentially toxic metallic wear nanoparticles and trace metal ions release from metal-on-metal orthopedic implants in the human biological specimens: an overview of in vivo and ex vivo clinical studies, World Journal of Advanced Research and Reviews 2020 (2020) 2581–9615, https://doi.org/10.30574/wjarr.
[57] V. Lautenbach, S. Hosseinpour, W. Peukert, Isoelectric point of proteins at hydrophobic interfaces, Front. Chem. 9 (2021), https://doi.org/10.3389/fchem.2021.712978.
[58] S.L. Hirsh, D.R. McKenzie, N.J. Nosworthy, J.A. Denman, O.U. Sezerman, M.M. M. Bilek, The Vroman effect: competitive protein exchange with dynamic multilayer protein aggregates, Colloids Surf. B Biointerfaces 103 (2013) 395–404, https://doi.org/10.1016/j.colsurfb.2012.10.039.
[59] E. Jurrus, D. Engel, K. Star, K. Monson, J. Brandi, L.E. Felberg, D.H. Brookes, L. Wilson, J. Chen, K. Liles, M. Chun, P. Li, D.W. Gohara, T. Dolinsky, R. Konecny, D.R. Koes, J.E. Nielsen, T. Head-Gordon, W. Geng, R. Krasny, G.-W. Wei, M. J. Holst, J.A. Mccammon, N.A. Baker, TOOLS FOR PROTEIN SCIENCE improvements to the APBS biomolecular solvation software suite, Protein Sci. 27 (2018) 112–128, https://doi.org/10.1002/pro.3280.
[60] A. Salis, M. Boström, L. Medda, F. Cugia, B. Barse, D.F. Parsons, B.W. Ninham, M. Monduzzi, Measurements and Theoretical Interpretation of Points of Zero Charge/Potential of BSA Protein 27 (2011) 11597–11604, https://doi.org/10.1021/la2024605.